

# Trajectory Optimization of Microgravity Atmospheric Flights Based on a Hybrid Heuristic Algorithm

Seyed M. Malaek<sup>1</sup> and Sina Moradi<sup>2</sup>

**Abstract** Due to the ever increasing space related missions, *Microgravity* condition during atmospheric flight is in great demand for astronauts training purposes. Perpetual in-orbit flights are impracticable to assimilate within the Earth's atmosphere; nonetheless, zero-G maneuvers have proven to be effective as a significant part of any space related program. In the absence of any specifically designed aircraft for zero-G flights, we could modify or adapt existing ones for such maneuvers. In this work, we use a systemic approach to demonstrate how we could develop a trajectory together with a control system to support zero-G flights for a given aircraft. We further show how the process could be generalized to partial gravity maneuvers, which Lunar and Martian gravity simulation comprise the focus of attention. In this article, the required inputs of an aircraft as a function of time for a near-optimal flight cycle is studied. The optimization procedure leading to proper elevator inputs has been carried out by two methods of Tabu Search and Continuous Ant Colony System, which has proven to be effective considering the governing constraints.

## 1 Introduction

The sense of weight refers to the distinct strain in the constituent particles of entities. However, it is well-known that the gravitational field of Earth exerts a body force that acts uniformly on all molecules of a given object. On the one hand, the natural source of such forces are unidentified and therefore, it is very hard to reconstruct such body forces with the desired intensities within the Earth's atmosphere. On the

---

<sup>1</sup> Prof. Seyed Mohamad Bagher Malaek

Flight Dynamics and Control Division at Aerospace Department of Sharif University of Technology, Azadi Street, Tehran, Iran, e-mail:[malaek@sharif.edu](mailto:malaek@sharif.edu)

<sup>2</sup> Sina Moradi (Student)

Flight Dynamics and Control Division at Aerospace Department of Sharif University of Technology, Azadi Street, Tehran, Iran, e-mail:[30na.moradi@gmail.com](mailto:30na.moradi@gmail.com)

other hand, there are quite a number of scientific activities that demand for weightlessness; for example, training astronauts on the planet Earth before sending them to the outer space. Consequently, it is quite logical to think of a systematic approach to create such conditions with the available tools. This work is an attempt to clarify the near-optimal process required to create microgravity conditions through well-defined trajectories conducted by an aircraft.

### ***1.1 Literature Review***

During the Second World War pilots experimentally acquainted with zero-G maneuvers. The so-called maneuvers later studied elaborately and the result was the invention of laboratories for astronauts training purposes. At first, it was confidential for years. Nevertheless, it gradually attracted the attention of many countries. However, the earliest published works on partial gravity flights go back in 1990s.

Benefiting from the nonlinear inverse dynamics technique, F. Mora-Camino and A. K. Achaibou analyzed the zero-G maneuvers in 1993 [4]. In that study, the aircraft was considered in a vertical plane with constant throttle setting during the maneuver [4]. This article represents a semi-linear form for aerodynamic coefficients and it considers the maneuver as the problem of driving the aircraft from a constant velocity level with the normal load factor equal to one, to the zero gravity flight in a way that the aircraft experiences a smooth alteration of load factor, which follows a first order differential equation [4]. Moreover, a state representation of the vertical flight dynamics considered, in which the input is the derivative of elevator, the output is load factor, and the states include velocity, flight path angle, angle of attack, pitch rate, and elevator [4]. Furthermore, mass uncertainty, thrust error with white noise, and air turbulence with Dryden model separately studied for the variation of the load factor throughout the maneuver.

Written by A. Peter Allan and the colleagues, a more detailed and specific study for the aircraft DC-9 to perform parabolic flights introduced in 1998 [5]. This work focuses on the design of a low-gravity flight director that aims for free floating and experiment inside the airplane [5]. In that case, the airplane tends to fly inside an imaginary tube that is only 60cm larger than the aircraft [5]. The study takes place in three dimensions and based on observations, it was revealed that the control power varies about linearly with speed for the elevator [5]. The same approach also considered for aileron and rudder but not for throttle [5].

Later in 1999, utilizing a gain scheduler, a predictor, and a sequencer, a general approach for flight director design of the zero-G maneuvers introduced by Ruud J. A. W. Hosman and Robert C. Kunen [2]. Thanks to the Technical University of Delft for this work and the succeeding ones. The study aims to maintain the pilot's gain constant. Moreover, the characteristics of the aircraft approximated by a second order system with the damping and bandwidth of short period mode [2]. This is because in the range where the pilots control the aircraft, the Bode diagram of the

transfer function of load factor to elevator input shows an almost constant magnitude with small phase angle.

Afterwards, a precious article prepared by A. M. (Alwin) Kraeger and M. M. (René) van Paassen on micro- and partial gravity atmospheric flight proposed in 2002 [3]. The control concept of this work intends for solving the problem of parabolic flights almost in real-time. Therefore, the pilot is not obliged to follow a certain predefined trajectory [3]. In other words, the nominal trajectory is not unique and the perturbed aircraft states are considered as the new initial condition to engender a new trajectory [3]. Here, the definition of limitation by introducing the time intervals of  $\Delta t$ , together with the crucial assumption of the cancelation of thrust and drag forces, make the study reliable, accurate, and easily usable [3]. Furthermore, thirteen types of control feedback strategies studied in this article, which revealed that the best result happens when utilizing the error signal of pitch rate and its reference measurement [3].

Written by J. M. M. van den Heuvel and the colleagues in 2008, and by B. Maselink and the co-authors in 2009, two consecutive articles on flight director design of partial gravity flights that complement each other were published [6, 9]. The use of linearization plays an important role in these works. Moreover, the studies conducted on the Bode plots of the airplane's transfer function of pitch rate and load factor to elevator input, demonstrates that McRuer crossover frequency model is advantageous in order to minimize the pilot's control effort [6, 9]. This model states that pilots performing compensatory tasks adapt their behavior to the whole dynamic system including the pilot itself [6, 9]. This adaptation is in a way that the open loop of the dynamic system near the crossover frequencies resembles a single integrator and a time delay [6, 9].

## ***1.2 The Purpose of the Concurrent Research***

Scientifically, orbiting spacecraft around Earth is continuously freefalling toward it at a constant altitude with an identical curvature with respect to that of Earth. Freefall is a situation when the sole force applying on an object is due to the placement in a uniform gravitational field. Therefore, the lack of contact forces obscure the weight. An ideal microgravity is hypothetical indeed, but by traversing a parabola, while nullifying the air resistance [3, 6, 9], a high level of accuracy is accessible even in atmospheric flights. Having simply considered a fixed downward gravitational field of Earth, a premeditated parabolic flight can engender microgravity during a short period of virtual atmospheric freefall. Partial gravity flights, fashionably Lunar and Martian, also follow the same principle.

In parallel with training astronauts, there are also vital materials and amalgams that should form homogeneously and call for weightlessness condition. As an example, we could name precious compounds like Interferon, a life-saving drug for

cancerous cases [10]. Parabolic flights provide a simulated microgravity environment for the scientists to study the potential of experimenting in an orbital everlasting microgravity situation. Surprisingly, conventional airplanes designed for a different purpose than zero-G laboratories perform the current parabolic flights.

Due to the importance of the zero-G flights, it is expected a new generation of aircrafts, which is mainly designed for such purposes, to emerge in near future. Such class of aircraft must be able to support astronauts training with meaningful durations of weightlessness to optimize the quality and cost. However, in the absence of these specific aircrafts, we can rely on the conventional airplanes to support zero-G maneuvers. Obviously, the existing types mostly suffer from the inability to compensate for the loss of kinematic energy while climbing. Besides, the maximum operating speed suppresses the airplane's capability to perform lengthier parabolic trajectories. Thus, subsonic aircrafts, which are designed to fly at Mach numbers lower than one to save as much fuel as possible and to abstain sound booms, may not be suitable for zero-g flights at all.

It is quite clear that the budgets allocated for space-based explorations and even trips to Mars, clearly justify the investment to design and build an aircraft with tailored missions and programs for training astronauts. This work, in its simplest form, aims to describe a systematic approach to perform near-optimum parabolas; therefore, we aim to prepare a template that assays the potential of various airplanes of different classes to perform zero-G maneuvers.

In the concurrent article, the necessary steps to implement a complete near-optimal microgravity atmospheric flight has prepared in a comprehensive way. Generally, a typical cycle divides into different segments that are (1) Cruise Flight, (2) Pull-up, (3) Transition to Zero Gravity, (4) Microgravity, and (5) Safe Exit.

## **2 Kinematics and Dynamics of Parabolic Flights**

The standard deviation of acceleration across the airplane in the body frame of reference is negligible compared to the magnitude of it at the aerodynamic center [6, 9]. Consequently, a point mass model is applicable. Therefore, the nominal trajectory of an aircraft in a microgravity flight is generally defined by the kinematics of a projectile in the lack of air resistance, since no contact force is desired in freefall.

### ***2.1 The Kinematics of Quasi-Parabolas***

The generalized quasi-parabola trajectory is represented in Fig. 1. Whether the maneuver is a parabola for microgravity or a quasi-parabola for partial gravity, in the body frame of reference, a supposed accelerometer tangent to the path always shows

zero. However, in the perpendicular direction, the presumably measured accelerations are zero and  $-\lambda g$  for weightlessness and altered gravity, respectively.  $\lambda$  is a non-negative specific force parameter equal or less than one [3, 6, 9]. The accelerometer measurements are non-gravitational. Therefore, while transforming the accelerations in the body frame of reference to that for Earth, gravity should be considered. Consequently, Eq. (1) describes the accelerations in the inertial reference frame of Earth, or mathematically the second derivative of trajectory. Unsurprisingly, for  $\lambda=0$  in the partial gravity trajectories, the equations for microgravity is obtained. Hence, microgravity is a special case for the solution of altered gravity. In other words, a quasi-parabola with  $\lambda=0$  is a parabola. The most popular partial gravity flights are Lunar gravity with  $\lambda=0.16$  and Martian with  $\lambda=0.38$ .

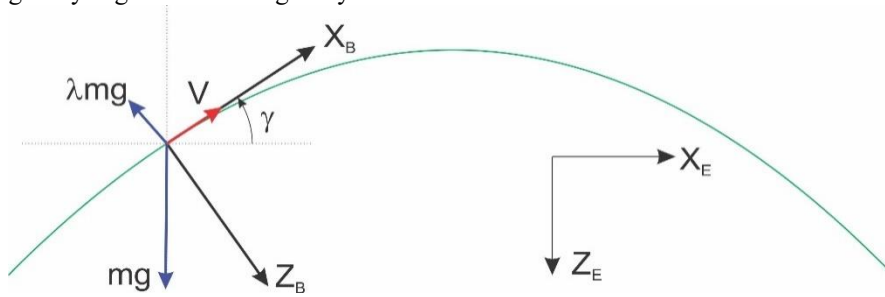


**Fig. 1.** The general trajectory of a projectile in partial gravity

$$\ddot{X}^E = -\lambda g \sin(\gamma) \quad , \quad \ddot{Z}^E = g - \lambda g \cos(\gamma) \quad (1)$$

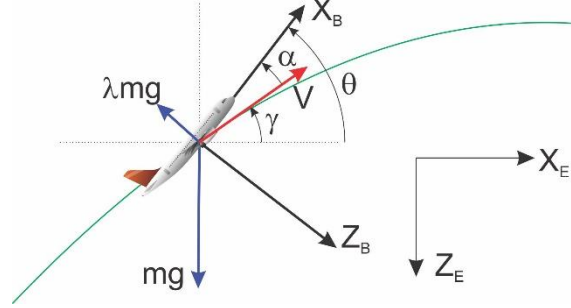
When  $\lambda=0$ , by integrating the Eq. (1) for any combination of initial states ( $V_0, \gamma_0$ ), the parameters of  $V(t)$ ,  $\dot{\gamma}(t)$  and  $\ddot{\gamma}(t)$  can be defined to determine the projectile motion. The calculations are available at [3], except that in our calculations, the direction of  $Z^E$  is downward. However, when  $\lambda \neq 0$ , the acceleration in the inertial frame is a function of path angle. Therefore, it is arduous to find an analytical solution for  $V(t)$ ,  $\dot{\gamma}(t)$ , and  $\ddot{\gamma}(t)$ . Instead, the path can be traced with the instantaneous amounts of these parameters. Hence, limitation techniques are advantageous.

## 2.2 The Dynamics of an Aircraft in Partial Gravity Maneuvers

In order to perform the maneuver by an airplane, the pilots should continuously nullify the drag force with the thrust, and simultaneously keep the load factor equal to the specific force parameter  $\lambda$  [3, 6, 9]. Definitely, this rule for thrust applies when the angle of attack,  $\alpha$ , is comparatively small. Fig. 2 shows an airplane traversing a quasi-parabolic trajectory to experience partial gravity in general. In this figure  $\alpha$  is the angle of attack and  $\theta$  represents the airplane's pitch angle. Thrust and drag forces

are absent due to the cancellation. Moreover, the study conducted in a two-dimensional plane, since the lateral-directional forces are negligible.

**Fig. 2.** Free diagram of an airplane performing a partial gravity maneuver



The drag force mainly varies with the change of dynamic pressure, and it is a minor contribution to apply the throttle accurately. Because the order of magnitude of the acceleration tangent to the path is much lower than that perpendicular to it. Therefore, while throttle adjustment is also considered, the focus is to control the load factor to follow  $\lambda$  during the maneuver.

Now Eq. (1) for freefall of a projectile turns into Eq. (2) [6]. This equation is the accelerations of an aircraft in the inertial frame of reference when performing partial-G maneuvers in general.

$$\ddot{X}^E = -\lambda g \sin(\theta) \quad , \quad \ddot{Z}^E = g - \lambda g \cos(\theta) \quad (2)$$

For a known specific force parameter  $\lambda$ , this equation reveals that while the time history of the aircraft's pitch angle is available, the accelerations are calculated. Therefore, as represented in Eq. (3), it is crucial to calculate the reference pitch rate of the airplane,  $q_{ref}$ , in a partial-G trajectory. Note that the subscripts 0 and  $(t=0)$  refer to the instant amounts in this equation and the subsequent ones. Moreover, by considering the instantaneous velocities in each direction that are contingent upon the flight path angle not the pitch angle, it is feasible to integrate Eq. (2) and find the trajectory.

$$\left. \begin{array}{l} \theta = \gamma + \alpha \\ q = \dot{\gamma} + \dot{\alpha} \end{array} \right\} \Rightarrow q_{ref} = \dot{\gamma}_{(t=0)} + \dot{\alpha}_{(t=0)} \quad (3)$$

### 2.2.1 Calculation of $\dot{\gamma}_{(t=0)}$

Benefiting from the definition of limitation while integrating Eq. (2), since instant velocities in each direction is determined, both the derivatives of velocity and flight

path angle are obtainable and correspond to the Eq. (4) and (5). The approach for this calculations is discussed in [9].

$$\dot{V}_{(t=0)} = -\lambda g \sin(\theta_0) \cos(\gamma_0) - (g - \lambda g \cos(\theta_0)) \sin(\gamma_0) \quad (4)$$

$$\dot{\gamma}_{(t=0)} = \frac{\dot{\gamma}}{V} \begin{pmatrix} \lambda \cos(\gamma_0) \cos(\theta_0) \\ +\lambda \sin(\gamma_0) \sin(\theta_0) \\ -\cos(\gamma_0) \end{pmatrix} \quad (5)$$

### 2.2.2 Calculation of $\dot{\alpha}_{(t=0)}$

To calculate the derivative of angle of attack is a major step toward finding the reference pitch angle. Although it is preferable not to exploit a linear aerodynamic assumption in the varied conditions of partial gravity maneuvers, it is still working almost flawlessly for the derivative of  $\alpha$ .

$$C_L = C_{L_0} + C_{L_\alpha} \alpha + C_{L_q} q + C_{L_{\delta e}} \delta e + C_{L_{i_H}} i_H \quad (6)$$

$$\alpha = \underbrace{\frac{\lambda mg}{\bar{q} S C_{L_\alpha}}}_{term1} - \underbrace{\frac{C_{L_0}}{C_{L_\alpha}}}_{term2} - \underbrace{\frac{C_{L_q}}{C_{L_\alpha}} q}_{term3} - \underbrace{\frac{C_{L_{\delta e}}}{C_{L_\alpha}} \delta e}_{term4} - \underbrace{\frac{C_{L_{i_H}}}{C_{L_\alpha}} i_H}_{term5}$$

$$\dot{\alpha} = \frac{d}{dt} (term1 - term2 - term3 - term4 - term5)$$

Ideally, the derivatives of the terms 2 and 5 are zero because they are constant. For the term 4 we have:

$$\left. \begin{aligned} \frac{d}{dt} (term4) &= \frac{C_{L_{\delta e}}}{C_{L_\alpha}} \frac{d}{dt} (\delta e) \\ \frac{C_{L_{\delta e}}}{C_{L_\alpha}} &\ll 1 \\ \frac{d}{dt} (\delta e) &\ll 1 \end{aligned} \right\} \Rightarrow \frac{d}{dt} (term4) \approx 0$$

By studying the European Space Agency (ESA) Parabolic Flights, it was observed that the pitch angle linearly varies during the maneuver. Thus, the pitch angle derivative is near constant and its second derivative is almost zero. Therefore:

$$\frac{d}{dt}(\text{term 3}) = \frac{C_{L_q}}{C_{L_\alpha}} \dot{q}, \dot{q} \approx 0 \Rightarrow \frac{d}{dt}(\text{term 3}) \approx 0$$

$$\dot{\alpha} \approx \frac{d}{dt} \left( \frac{\lambda mg}{\bar{q} S C_{L_\alpha}} \right) = - \frac{4 \lambda mg}{\rho S C_{L_\alpha}} \left( \frac{\dot{V}}{V^3} \right) \quad (7)$$

Consequently, by substituting the instant velocity and its derivative from Eq. (4) into the Eq. (7), Eq. (8) concocts.

$$\dot{\alpha}_{(t=0)} \approx \frac{2 \lambda mg^2}{\bar{q} V S C_{L_\alpha}} \left\{ \begin{array}{l} \lambda \sin(\theta_0) \cos(\gamma_0) \\ + (1 - \lambda \cos(\theta_0)) \sin(\gamma_0) \end{array} \right\} \quad (8)$$

### 2.2.3 The Reference Pitch Rate and Controlling Logic

Shown in Eq. (9), by adding Eq. (5) and (8), the equation for the reference pitch rate derives. Thus, based on the required measurements and feedbacks, the main skeleton for automatically controlling the airplane can be formed [3].

$$q_{ref} = \frac{|\rho c|}{V} \left( \begin{array}{l} \lambda \cos(\gamma_0) \cos(\theta_0) \\ + \lambda \sin(\gamma_0) \sin(\theta_0) \\ - \cos(\gamma_0) \end{array} \right) + \frac{2 \lambda mg^2}{\bar{q} V S C_{L_\alpha}} \left\{ \begin{array}{l} \lambda \sin(\theta_0) \cos(\gamma_0) \\ + (1 - \lambda \cos(\theta_0)) \sin(\gamma_0) \end{array} \right\} \quad (9)$$

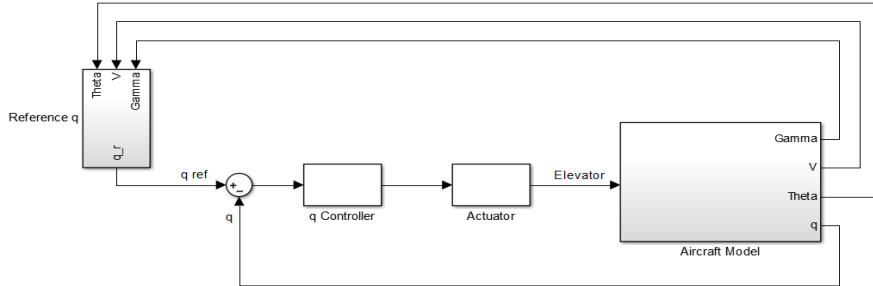


Fig. 3. Pitch rate controller logic

The reference pitch rate is a function of speed, pitch angle, and flight path angle. Hence, as shown in Fig. 3, a feedback from the so-called states are required. Moreover, the pitch rate's feedback is also needed in order to calculate the output error with the desired value of it. Correspondingly, the proper elevator input to obviate the unfavorable error applies and keeps the airplane in the desired trajectory.

To achieve the maximum possible time and a high level of accuracy in microgravity atmospheric flights means to push the aircraft to its limits. Flying near the maximum airplane's capabilities is a task better to be done by a computer instead of a human. Yet, the conventional airplanes currently carrying out parabolic flights are built for transportation purposes. These traditional aircrafts rely on a flight director with the same logic in controller design. Therefore, the pilot's accuracy improves while performing the compensating task of following the desired trajectory.

### 3 The Complete Near-Optimal Flight Cycle

Fig. 4 generally shows a complete cycle of microgravity (or partial gravity) maneuver for an airplane. The phases are analyzed separately since they are peculiar, but they are finally integrated to ensure the continuity of the subject. Each piece requires a particular dynamic based cost function that should be optimized. In order to define proper cost functions, we benefited from some techniques presented in [8].

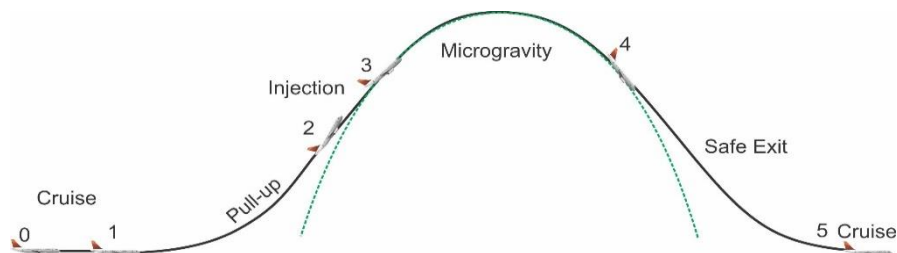


Fig. 4. A complete microgravity flight cycle

#### 3.1 Flight Phase Definition

The flight phases in Fig. 4 exhibit the regular procedure to perform altered gravity maneuvers. Designed with the intention to capture the maximum time intervals of the zero-G parabolas or the partial-G quasi-parabolas, the duration is mainly influenced by the cruise speed and significantly with the time to terminate pull-up. Subsequently, the description of phases is introduced.

### 3.1.1 Cruise

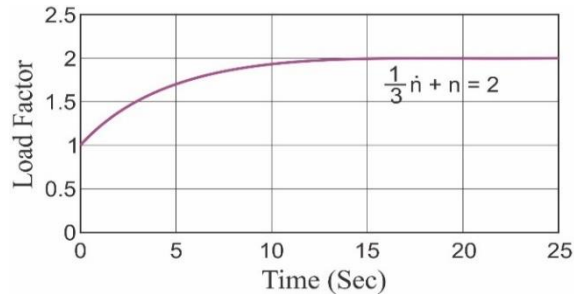
In this phase, the load factor is equal to 1 and the airplane states, such as angle of attack, flight path angle, speed and altitude remain unchanged. Flying in high altitudes to reach less turbulence air layers with velocities near maximum operating speed is recommended [5].

### 3.1.2 Pull-up

Here, the goal is to increase the path angle of the airplane accompanied by the lowest possible decline of the kinematic energy. Obviously, a sudden change in load factor is not applicable. Therefore, as shown in Eq. (10), using a first order differential equation for the increment of load factor can be an asset for a smooth pull-up [4]. Moreover, inspired from a set of available data for Zero-G Airbus A300 of ESA,  $\tau = 1/3$  is selected, which seems to fit the current level of industry's achievement. Therefore, Fig. 5 exhibits the desired load factor during pull-up for a conventional airplane. The principal goal in pull-up is to properly minimize the load factor's standard deviation from its desired value. Albeit the maximum allowable load factor is 2.5 for a conventional jet airplane, it is here bounded to a maximum of 2 for safety reasons. It should be mentioned that the airplane can pull-up until the stall angle of attack is reached, which usually occurs around 8 degrees in conventional aircrafts.

$$\tau \dot{n} + n = n_{desired} \quad (10)$$

**Fig. 5.** Anticipated behavior of load factor during pull-up



It worth noting that when the elevator is applied at point 1, the altitude drops slightly. This is because the aircraft is a non-minimum phase system and before any appearance of nose-up condition, it experiences loss of lift.

### 3.1.3 Injection

The injection phase precedes partial-G maneuver and proceeds pull-up. The responsibility of this phase is to match the airplane's path with the intended parabola. By

using the ESA Zero-G Flights as a benchmark<sup>3</sup>, a 7-second injection for microgravity flight, as well as, 6 and 5 seconds respectively for Lunar and Martian gravity defined.

At the termination of injection, the load factor should have already reached the desired value and its derivative should almost equal to zero. In addition, the aircraft must have enough tendency to maintain the target load factor when it instigates the microgravity<sup>4</sup> phase. To resolve, the simulation time for injection was added 2 seconds. In other words, the cost function defined purposely so that the final 2 seconds oblige the airplane to follow the desired load factor  $\lambda$ . For instance, the injection is in reality 7 seconds for microgravity maneuver, while the simulation runs for 9 seconds. But, the initial states to commence microgravity is taken from the seventh second of simulation.

### 3.1.4 Microgravity

Although phase four or the parabolic flight is the most important segment, it is the easiest one to define. Time of the simulation is given, since the kinematics of the airplane and a projectile are equivalent. Furthermore, cost function aims to maintain the load factor constant by minimizing the standard deviation from  $\lambda$ .

### 3.1.5 Safe Exit

The exit phase is crucial. The pilot should level the diving aircraft in-time without exceeding stall angle, maximum operating speed and maximum permissible load factor, assuming no elevator saturation occurs [2]. In fact, here we have selected a suitable dynamic based cost function that helps to avoid reaching the respecting boundaries of velocity, load factor, and angle of attack [8].

## 3.2 Throttle Adjustment

The acceleration tangent to the path should be controlled properly. The throttle setting is in general between idle at 0.5 and a maximum that engine specification allows. We are required to select the maximum engine power in a way to avoid overheating while maintaining the safety of flight. Thus, the maximum power assigned to the throttle is considered 1.1; however, throttle cannot surpass 1.0 during the optimization. A simple trend for throttle setting was yielded by analyzing the operating velocity. This attitude can be applied to various conventional airplanes.

---

<sup>3</sup> <https://www.youtube.com/watch?v=7g01pIgsfXk&feature=share>

<sup>4</sup> Partial Gravity in General

In this work, we first find the proper throttle setting for the cruising flight. For the second leg of the maneuver, we command to increase the setting with a moderate slope until it saturates at maximum for the rest of pull-up phase. It is interesting to note that during injection, the airplane experiences a sharp reduction of thrust to near-idle. Whereas in altered gravity phase the dynamic pressure is almost quadratic, a linear drop of throttle symmetrical to the apex with idle thrust, is almost satisfactory to nullify the existing drag. For the safe exit phase, however, the airplane is in diving mode and therefore, we keep the throttle constant until the aircraft's flight path angle recovers. The later introduced Fig. 10 in section 3.5.1 helps to understand the concept.

### ***3.3 The applied Heuristic Optimization Tool TCACS***

Having demonstrated in [7], TCACS is an optimization tool for minimizing continuous multi-minima functions. This combinatory optimization method utilizes Tabu Search (TS) and Continuous Ant Colony System (CACS). Inspired from the nature, CACS algorithm deals with virtual pheromone<sup>5</sup> distribution for some imagined ants. Therefore, as the amount of pheromone increases, it is more likely for the ensuing ants to be guided toward the optimum solution that minimizes an intended cost function. Finally, by continuing this process, a convergence takes place in the direction of the best solution. Succinctly, the method of Continuous Ant Colony System is the foundation of our tool, and the pheromone model is based on Gaussian probability distribution [7], which the details are not much relevant to the concurrent article and the interested reader can find specific information in [7].

To improve the convergence rate and reduce the computational costs, TS is hybridized with CACS to result TCACS. The basis of this algorithm comprises three recurring levels. At first, the ants are uniformly distributed in the search space and the cost function is evaluated. Then, a Promising List [7] is formed that comprise the best solutions, as well as a Tabu List [7] for the worst ones. During the iterations, TS quickly detects Hypersphere Tabu Balls [7] on our n-dimension search space, which they do not contain our optimum solution. Afterwards, while preventing improper regions, the pheromone distribution is updated [7]. Finally, the iterating process winds up if the predefined stopping condition is met. Fig. 6 helps to understand how TCACS works.

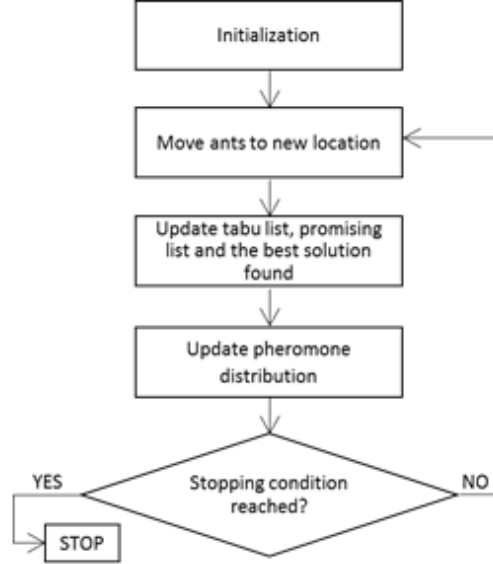
This heuristic method is utilized to figure out the near-optimal elevator. We believe that the application of TCACS in zero-G maneuvers is a minor contribution. We do not have insist on the algorithm used for the optimization, except that according to [7] TCACS has shown to be superior to eight other evolutionary approaches in solving standard benchmarks. It is also fast, accurate, and reliable to

---

<sup>5</sup> A chemical substance produced and released into the environment by an animal, especially an insect, affecting the behavior of others of its species.

find the global minimum and it never traps inside a local minimum region. However, it is completely true that any other powerful optimization algorithm can also be utilized.

**Fig. 6.** General flowchart of TCACS [7]



### 3.4 Optimization

Here, the main goal is to minimize the deviation of load factor from its desired value. Exhibited in Eq. (11), the required elevator for each segment can be defined as a polynomial function of time with coefficients  $P_1$  to  $P_n$ . The coefficients are the multiple inputs for the hybrid heuristic algorithm with their lower and upper search bounds logically set.

$$\delta e = P_1 t^n + P_2 t^{n-1} + \dots + P_{n-1} t + P_n \quad , \quad \begin{cases} P_{1_L} \leq P_1 \leq P_{1_U} \\ P_{2_L} \leq P_2 \leq P_{2_U} \\ \vdots \\ P_{n_L} \leq P_n \leq P_{n_U} \end{cases} \quad (11)$$

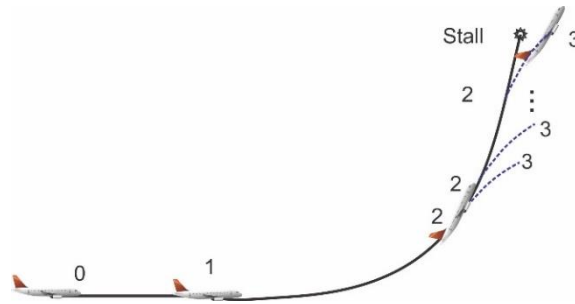
At the start of each segment when time is zero, the elevator equals to  $P_n$ . At the beginning of each leg, the algorithm selects  $P_n$  equal to the elevator deflection at the termination of the previous leg. This can be done by almost overlaying the lower

and upper bound of the search margin for  $P_n$ . Moreover, to ensure the integrity of the maneuver, the aircraft states, namely speed, altitude, pitch angle, pitch rate, and angle of attack must be precisely the same for the final time of a mission leg and the initial time of the next.

A trimmed cruise flight exhibits consistent states, as well as constant inputs for throttle and elevator. Utilizing a proper cost function, TCACS can trim the aircraft by tuning initial states and both inputs. On the one hand, lower altitudes are more susceptible to air turbulence, on the other hand, the maximum service ceiling constrains the maneuver. Therefore, the cruise altitude should be chosen in a way that the aircraft flies near the service ceiling at the top of the parabola.

Afterwards, at the given altitude and velocity, the predefined pull-up phase carries out. The ultimate pull-up time refers to the longest pull-up until the aircraft stalls. During pull-up, multiple imaginary injections to the corresponding parabola is performed until the airplane runs into the ultimate condition of stall. Since the airplane is tending to follow a projectile trajectory in the main maneuver, time of the microgravity leg can be predicted using the terminating states of the third leg, namely  $(V_3 \ \gamma_3)$ , which are the same as the initial states of fourth leg. Fig. 7 helps to visualize the approach utilized to uncover the optimum microgravity time.

**Fig. 7.** Performing multiple injections to find the best Pull-up Time



In the fourth leg of optimization, the energy is almost conservative. Therefore, the increase of altitude to the apex is accompanied by the decrease of speed. Thus, the distance between initial and final positions in a time interval is minimum at the apex, and drastically increases with the growth of flight path angle. Moreover, the behavior of the velocity vector is symmetrical with respect to a horizontal plane. Therefore, at the same altitude the airplane experiences identical true airspeed, while climbing and diving. Consequently, in order to capture the maximum amount of time intervals, the partial gravity trajectory should be evenly shaped in theory.

According to Eq. (1), Fig. 8 is the partial gravity time surfaces for an object with a symmetrical path that initiates the trajectory with an arbitrary velocity and path angle. The modeling was done with the help of Simulink MATLAB, which revealed similarities with [6]. In Fig. 8a it is clear that at a given velocity, the microgravity time continuously rises with the growth of initial path angle to 90 degrees. However, in Fig. 8b and 8c, the story is different. For Lunar gravity simulation, the optimum time looks to happen around 74 degrees of path angle and it is almost 59 for Martian.

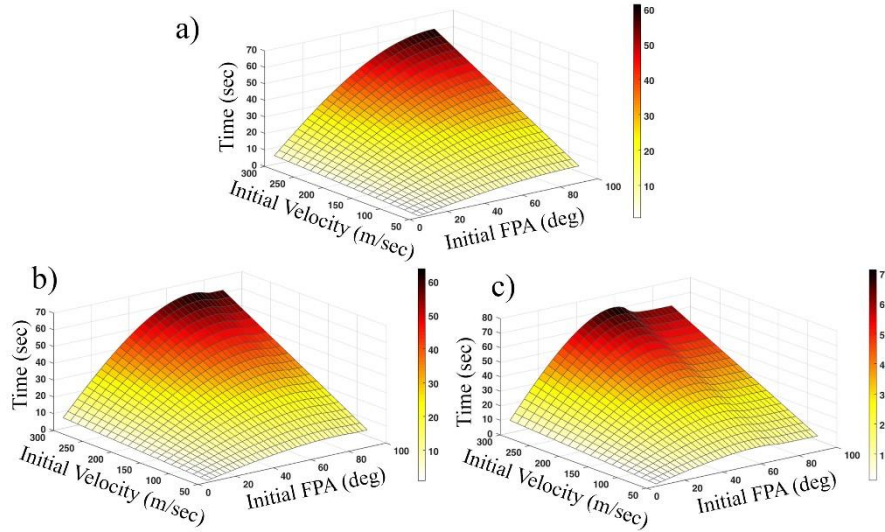


**Fig. 8.** Time Surface for Initial States. a) Microgravity b) Lunar Gravity c) Martian Gravity

To perform the maneuver optimally, the best combination of  $(V_3 \ \gamma_3)$  at point 3 on Fig. 7 should be figured out. Considering all of the possible injections to the altered gravity maneuver, distinct points on the time surfaces of Fig. 8 can be located. Having traced these points, a peculiar curve reveals on the surfaces. The objective is to find the combination of  $(V_3 \ \gamma_3)$  at the absolute extremum of these curves. Correspondingly, the optimum time to terminate pull-up is obtainable.

The safe exit phase initiates finally. The cycle is complete if the aircraft is able to recover from diving without reaching stall and more importantly, without exceeding the maximum allowable velocity and load factor. Otherwise, an arbitrary time interval is considered to shorten the end of fourth leg and initiate the exit phase until the recovery is performed safely.

### 3.5 Case Studies

The prepared algorithm is capable of calculating the near-optimal inputs to maximize the duration of the intended maneuver, whether it is microgravity, Lunar or Martian gravity. By substituting the aerodynamic characteristics of few airplanes, which are available at [1], the utilized simulation originated from Airlib<sup>6</sup>. Satisfying results obtained for the aircrafts with different characteristics, namely the Boeing 747

<sup>6</sup> Written by Marc Rauw and available at the matlabcentral website, Airlib is a library of nonlinear aircraft models

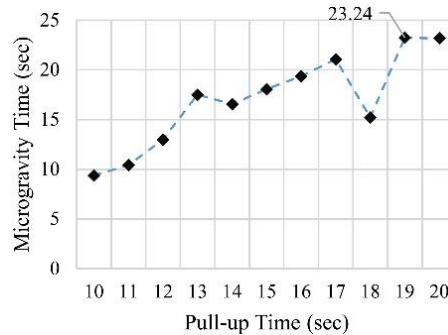
and the Learjet 24. Here, since the current zero-G airplanes are wide-body jets, this study focuses on microgravity maneuver for the Boeing 747.

### 3.5.1 The Boeing 747 in Microgravity

The investigation of flying at low speeds and altitudes for the first leg is vain. Higher altitudes are less potential to air turbulence and the airplane should fly close to the maximum operating velocity to store as much kinematic energy as possible. Studying the altitude variation of zero-G Airbus A300 and the service ceiling of B747, resulted in choosing the flight level of 30,000 feet (FL30) for the cruise leg. The airplane's maximum operating velocity is Mach number of 0.92, which at this altitude results in true air speed of 281 meters per second. However, for safety reasons the cruise speed selected equal to 275 meters per second.

In the second leg, B747 stalls after 21 seconds of pull-up. However, we should determine a proper termination time for this leg. In addition, there is no merit in starting the injection phase soon after the aircraft initiates pull-up. Hence, to study the possible injections, the first 10 seconds of pull-up is excluded. Therefore, having arbitrarily considered time intervals of one second, 11 possible injections from 10 to 20 seconds carry out. Performing each injection will result in a specific combination of  $(V_3 \ \gamma_3)$ . For each of these 11 points, the corresponding altered gravity time is checked on Fig. 8, which are sketched in Fig. 9. This figure exhibits that terminating pull-up after 19 seconds provides the near-optimum microgravity time.

**Fig. 9.** Zero-G duration corresponding to the airplane pull-up time



Consequently, to optimally reach point 3 on Fig. 4, the Boeing 747 should fly a total of 36 seconds including an arbitrary 10-second cruise, followed by a 19-second pull-up and a 7-second injection to microgravity. In this case, Fig. 8a offers a 23.24 second microgravity for the phase four.

The flight cycle is over if the safe exit accomplishes. Otherwise, the arbitrary time interval of 0.2 seconds is considered to reduce the termination time of the fourth leg and initiate the exit phase until recovery is performed safely. It takes 6 iterations or 1.2 seconds for the Boeing 747 to finally perform a safe exit to the cruise flight. Thus, the actual microgravity time would be almost 22 seconds. Therefore, from 36 to 58 seconds, the aircraft fulfills the intended parabolic maneuver to

create the sense of weightlessness. Subsequently, for a thorough microgravity cycle from cruise to exit, the airplane's longitudinal inputs, accelerations in body frame of reference, and states are demonstrated in Fig. 10 to 12, respectively.

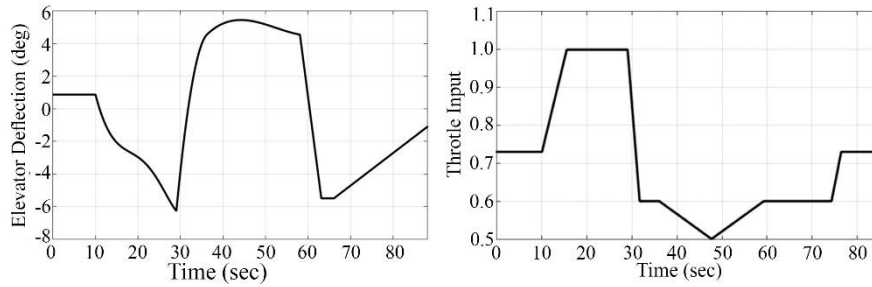


**Fig. 10.** Longitudinal inputs for a complete microgravity cycle

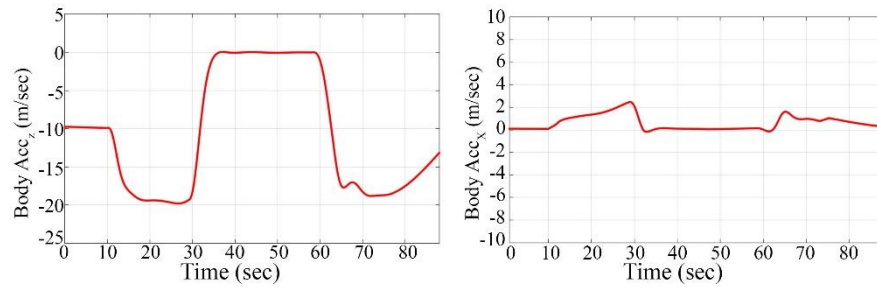


**Fig. 11.** Body accelerations for a complete microgravity cycle

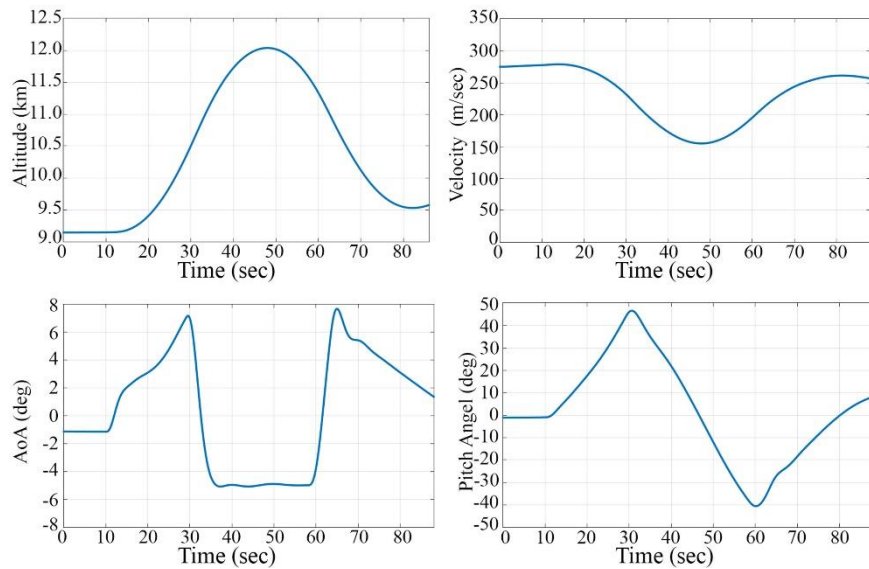


**Fig. 12.** Longitudinal states for a complete microgravity cycle

For the throttle input in Fig. 10 the explanation is in section 3.2. The elevator, however, is optimized and reveals a nearly quadratic behavior in microgravity. Note that a  $-5.5$  degree saturation is considered for the last leg to prevent stall.

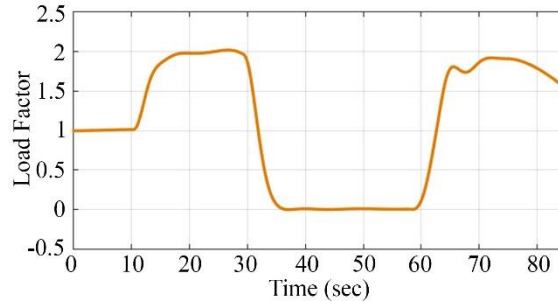
Fig. 11 represents body accelerations. The acceleration in x-direction does not exceed  $0.26g$ . Therefore, it is clear that the order of magnitude of the acceleration in x-direction is considerably lower than that in z-direction. More importantly, during microgravity, the aircraft's acceleration is almost zero in both directions, which validates the accuracy of maneuver.

Fig. 12 exhibits the states. Although the airplane strives to minimize the loss of velocity during pull-up, it still initiates microgravity leg with  $50.9\%$  of its kinematic energy at cruise. The rest of energy dissipates or turns into unserviceable potential energy. Loss of kinematic energy is extremely unfavorable in microgravity flights.

The altitude remains below the service ceiling and the microgravity leg starts at  $11271$  meters of altitude. The angle of attack almost covers its whole possible range in the near-optimal flight cycle. More importantly, as presented in Eq. 8, the angle of attack remains almost consistent in microgravity leg; however, it is domelike for partial gravities. Besides, the pitch angle varies almost linearly throughout the cycle.

The airplane's load factor is shown in Fig. 13. This figure reveals that the load factor remains in a safe and accurate region throughout the maneuver, while the maximum structural capability of the airplane is utilized.

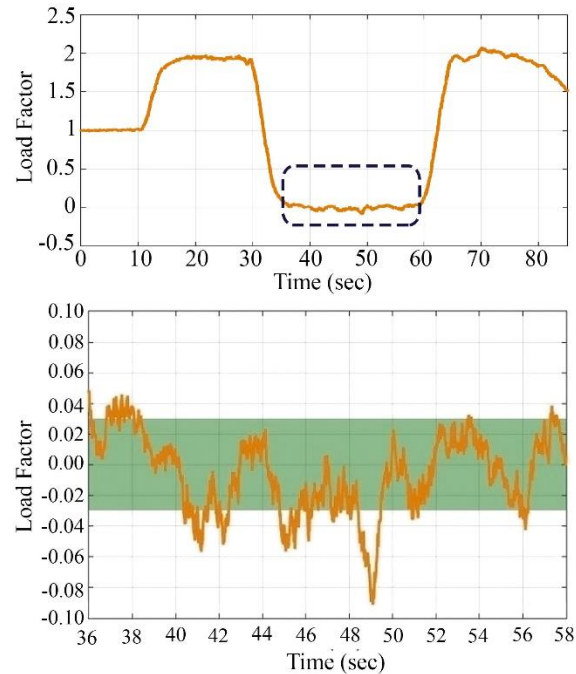
**Fig. 13.** Load factor for a complete microgravity cycle



### 3.5.2 The Influence of Air Turbulence on Zero-G Maneuver

Created by Dryden model in Simulink MATLAB, Fig. 14 shows the load factor of B747 during the near-optimal microgravity phase with the presence of air turbulence. The green region, which is considered  $\pm 0.03g$  [2], is an acceptable range of load factor for microgravity parabolic flights. Lucidly, intense atmospheric turbulences adversely affect the level of accuracy to an impracticable level.

**Fig. 14.** Load factor during microgravity with the presence of air turbulence



Obviously, among all five segments of a near-optimal parabolic flight cycle, it is the fourth leg or partial gravity in which the aircraft's sensitivity to air turbulence is crucial. Consequently, we should look for large airplanes capable of flying in higher altitudes.

#### 4 Conclusion

The studies conducted by the authors during the course of this project reveal that a purposefully designed *zero-G airplane* would have been the best approach to perform zero-G flights within the Earth's atmosphere. The supposed aircraft could be analogous to Concorde or TU-144. Benefiting from the concurrent template, although it deserves an in-depth investigation, the potential of these airplanes to become our new microgravity laboratories could be studied. Nonetheless, the Direct Operating Cost (DOC) of such supersonic aircrafts could be of a great concern. One point is quite obvious that the fleet of Concorde was forced out of service by managerial choice and that fleet deserves to be studied for a new application; such as microgravity flights.

## References

1. Roskam, J.: *Airplane flight dynamics and automatic flight controls*, Lawrence, third edition. Appendix B, pp. 479-550 Lawrence, KS: DARcorporation, (2001). ISBN 1-884885-17-9
2. Hosman, R., Kunen, R.: Flight director guidance throughout the parabolic maneuver, IEEE SMC99 Conference Proceedings. Conference on Systems, Man, and Cybernetics (Cat. No.99CH37028), pp. 1076–1081 (1999). doi: 10.1109/ICSMC.1999.815706
3. Kraeger, A., Paassen, R. V.: Micro- and Partial Gravity Atmospheric Flight, AIAA Atmospheric Flight Mechanics Conference and Exhibit, pp. 2–6 (2002). doi: 10.2514/6.2002-4499
4. Mora-Camino, F., Achaibou, A. K.: Zero-gravity atmospheric flight by robust nonlinear inverse dynamics, *Journal of Guidance, Control, and Dynamics*, vol. 16, pp. 604–606 (1993). doi: 10.2514/3.21056
5. Allan, A., Logsdon, K., Mcknight, R.: Low-gravity flight director for free-floating experiments - DC-9 testing, 36th AIAA Aerospace Sciences Meeting and Exhibit, pp. 1–4 (1998). doi: 10.2514/6.1998-453
6. Heuvel, A. V. D., Mulder, M., Paassen, M. V., Veld, A. I. T.: Design of a Partial Gravity Flight Director, AIAA Guidance, Navigation and Control Conference and Exhibit, pp. 2–13 (2008). doi: 10.2514/6.2008-7159
7. Karimi, A., Nobahari, H., and Siarry, P.: Continuous ant colony system and tabu search algorithms hybridized for global minimization of continuous multi-minima functions, *Computational Optimization and Applications*, vol. 45, pp. 639–661 (2008). doi: 10.1007/s10589-008-9176-7
8. Malaek, S., Kosari, A., and Jokar, S.: Dynamic based cost functions for TF/TA flights, IEEE Aerospace Conference, pp. 3–4 (2005). doi: 10.1109/aero.2005.1559479
9. Masselink, B., Veld, A. I. t, Mulder, M., and Paassen, R. V.: Design and Evaluation of a Flight Director for Zero and Partial Gravity Flight, AIAA Guidance, Navigation, and Control Conference, pp. 2–12 (2009). doi: 10.2514/6.2009-5987
10. Thomas, V. A., Prasad, N. S., Ananda Mohan Reddy C.: Microgravity research platforms - A study, Programme Planning and Evaluation Group, ISRO Satellite Centre, Airport Road, Bangalore 560 017, India, *CURRENT SCIENCE*, VOL 79, NO. 3, pp. 1-2, (2000)